Alizadeh, Mahdi; Radevici, Ivan; Li, Shengyang; Oksanen, Jani

Chemovoltaic effect for renewable liquid and vapor fuels on semiconductor surfaces

Published in:
ChemSusChem

DOI:
10.1002/cssc.202301522

Published: 08/03/2024

Document Version
Publisher's PDF, also known as Version of record

ChemSusChem

Research Article
doi.org/10.1002/cssc.202301522

Chemistry Europe
European Chemical Societies Publishing

www.chemsuschem.org

Chemovoltaic effect for renewable liquid and vapor fuels on semiconductor surfaces

Mahdi Alizadeh,*[a] Ivan Radevici,[a] Shengyang Li,[a] and Jani Oksanen[a]

The chemovoltaic effect – generation of electronic excitation by exergonic redox reactions – has been observed on metallic surfaces of Schottky junctions and is proving to be pivotal in explaining in detail the momentum conservation relations of chemically active collisions. As shown in this work, it can hold keys for direct chemical energy harvesting by semiconductor solar cells. To study the possibilities of chemovoltaic energy conversion by semiconductors, we have modeled and designed an 'electrolyte-free fuel cell' formed by a GaAs diode that can host electrochemical fuel oxidation and oxidant reduction reactions on its conduction and valence bands and as a result convert renewable chemical energy (as well as light) into electricity. The experimental results show that exposing the surface of a suitably designed solar cell to methanol liquid or vapor in the presence of oxygen or hydrogen peroxide leads to the generation of electrical power.

1. Introduction

Electrochemical processes involving redox reactions play a crucial role in a wide range of applications, spanning from fuel cells and electrolysis to photoelectrochemical and photocatalytic processes. The fundamental understanding of these processes lies in the realm of thermodynamics, which sets the most fundamental limits for the feasibility and efficiency of such reactions. Over the recent decades, the exploration of the chemovoltaic effect on metals has garnered significant attention due to the findings that the related surface reactions cannot be described by the usual Born-Oppenheimer approximations used in computational chemistry.[1,2] Recent discussions on the role of hot electrons on metal surfaces have shed light on this phenomenon, with numerous studies published in esteemed scientific journals.[3–5]

While the focus of these discussions primarily centers around metal surface chemisorption, it is important to recognize that similar thermodynamic principles are at play in the realm of energy conversion. Semiconductors, in particular, are of great interest in this context, as they play a crucial role in photoelectrochemical (PEC) processes and photocatalysis (PC). Following the first demonstration by Honda and Fujishima in 1972,[6] extensive efforts have been devoted on the idea of converting solar energy to storable chemical fuels such as hydrogen through water splitting[7–9] or organic fuels, such as methanol and ethanol, through photocatalytic hydrogenation of carbon dioxide.[10–13] The fuel generation in the PEC cells proceeds through three steps where the cell 1) absorbs an incident photon, 2) generates an electric current between the anode and the cathode and 3) drives a redox reaction producing e.g., H_2 and O_2 at the cathode and anode, respectively.

While the PEC fuel generation relies on a three-component cell consisting of two electrodes and an electrolyte, modern approaches for the PC hydrogenation and water splitting also include the possibility of using single component setups, where the fuel generation takes place e.g. on the surface of a nanoparticle.[14,15] Figure 1(a) schematically illustrates such a system for the hydrogenation of carbon dioxide.[16] In the PC system, incident light generates an excitation in the form of excess electrons and holes in the conduction and valence bands of the semiconductor acting as an independent virtual cathode and anode, which drive the hydrogenation reaction producing methanol at the surface of the particle.[15] Quite remarkably, the PC process has been shown to allow reaching a quantum efficiency (QE) of nearly 100% for water splitting when the H_2 and O_2 evolution reactions were catalyzed by Rh/Cr_2O_3 and CoOOH cocatalysts, respectively, on separate crystal facets of aluminum-doped strontium titanate ($SrTiO_3$:Al) photocatalysts.[17]

Considering the role of the virtual electrodes in the photocatalytic process, it becomes relevant to consider what happens if the directions of the redox reactions in Figure 1(a) are reversed. Figure 1(b) depicts this possibility in more detail, showing that with suitable changes in the energy levels and their alignments, methanol oxidation and oxygen reduction reactions result in the generation of electrons and holes on the semiconductor surface. In analogy with solar cells, the chemically excited electron-hole pairs can then be separated and transported to an external circuit, achieving the conversion of chemical energy into electricity using a single semiconductor electrode.

In this paper we first outline the fundamental thermodynamic relations governing the possibility of chemovoltaic energy conversion and then show that it is indeed possible to

[a] M. Alizadeh, I. Radevici, S. Li, J. Oksanen
Engineered Nanosystems Group, School of Science, Aalto University, Tietotie 1, Espoo, 02150, Finland
E-mail: mahdi.alizadehkouzehrash@aalto.fi

Supporting information for this article is available on the WWW under https://doi.org/10.1002/cssc.202301522

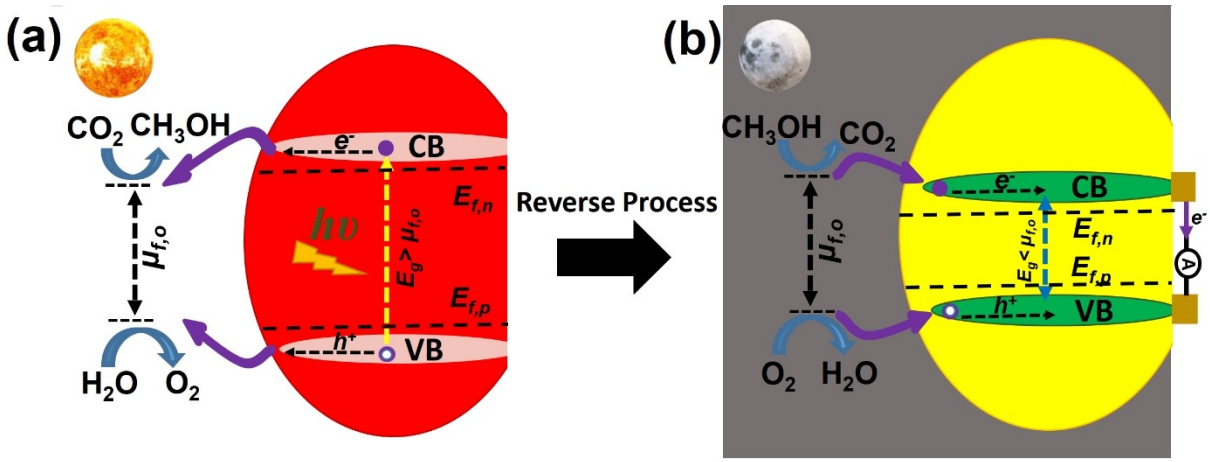

Figure 1. Operation principle of **(a)** solar-driven photocatalytic hydrogenation of carbon dioxide and **(b)** schematic illustration of the chemovoltaic effect in the dark, resulting from reversing the PC reactions at the semiconductor/non-ionic solution interface.

directly extract chemical energy from renewable fuels using GaAs based pn-junctions both in liquid and vapor phase.

2. Thermodynamic model of charge transfer at semiconductor/solution interface

The thermodynamics of redox reactions at semiconductor-liquid interfaces is well understood due to earlier interest in PEC and PC, especially through the works of Gerischer.[22–24] Figure 2 illustrates the most fundamental thermodynamics and charge transfer processes taking place at a semiconductor/solution interface, determined by the locations of the conduction and valence band edges (E_c, E_v), the quasi-Fermi levels of the electrons and holes (E_{fc}, E_{fv}) for the semiconductor (assumed to be in quasi-equilibrium) and the electrode potentials of the redox couple (E_f, E_o). The diagram also illustrates the cathodic and anodic decomposition potentials of the semiconductor[22] (E_{CD} and E_{AD}) and the role of reorganization energy (λ) responsible for the broadening of the energy levels of the redox couple.[20] Fuel oxidation reactions can take place through direct electron injection to the conduction band (arrow 1 in Figure 2(a)) or the associated cross reaction injecting electrons to the valence band (arrow 2). The oxidizer reduction reaction can equivalently take electrons from the valence band (arrow 3) or from the conduction band through the associated cross reactions (arrow 4). In the notation of this paper, positive currents are chosen to denote electron injection into the semiconductor. Figure 2(b) illustrates the more specific band diagram for a GaAs pn-junction and the energy levels of methanol + oxygen and methanol + hydrogen peroxide. As indicated in the figure and shown later in this paper, the methanol oxidation (MO) is expected to primarily proceed

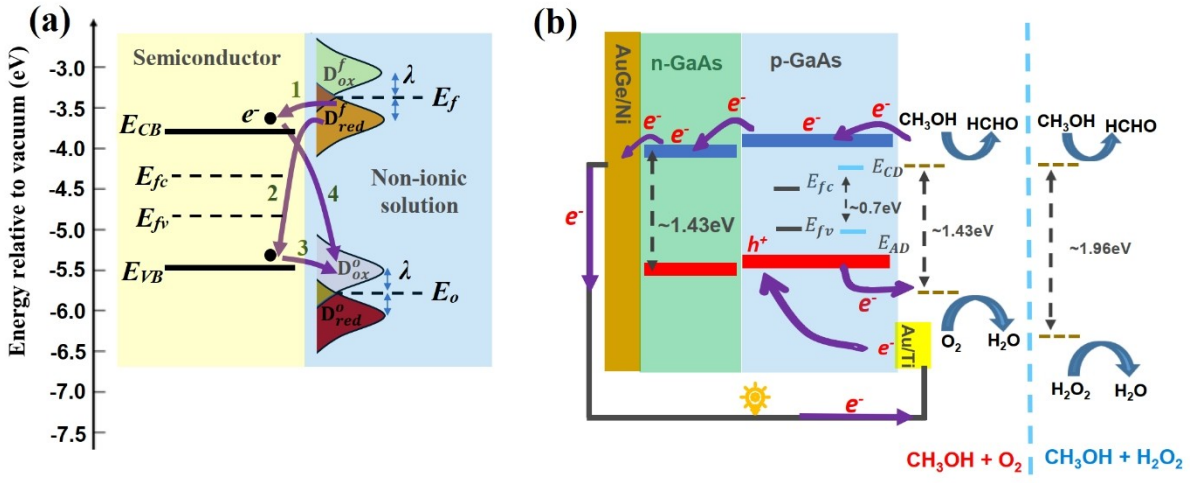

Figure 2. **(a)** The fundamental charge transfer processes present at a semiconductor/solution interface. **(b)** A schematic band diagram for a GaAs pn junction in contact with $CH_3OH + O_2$ and $CH_3OH + H_2O_2$ solutions, also showing the estimated band alignments for the respective redox potentials at standard conditions and the cathodic and anodic decomposition potentials E_{CD} and E_{AD} of GaAs.

through the conduction band of the GaAs surface and the oxygen or hydrogen peroxide reduction (OR and HPR) through the valence band. The fundamental thermodynamics of the cells are determined by the locations of the quasi-Fermi levels and the energy levels listed in Table 1. When the quasi-Fermi level of the electrons is below the electrode potential of the methanol oxidation reaction, methanol can provide electrons to the semiconductor as described by the half reaction

$$\begin{aligned} &CH_3OH\ (aq) \\ &H_2CO\ (aq) + 2H^+ + 2e^- \\ &E_{ox}\ = -0.2\ \text{V vs NHE.} \end{aligned} \tag{1}$$

Similarly, when the quasi-Fermi level of the holes at the GaAs surface is higher than the electrode potential of the O_2 or H_2O_2 reduction reactions, holes are injected into the semiconductor through the following half reactions, respectively:

$$\begin{aligned} &O_2\ (g) + 4H^+ \\ &2H_2O + 4\ h^+ \\ &E_{red}\ =\ 1.23\ \text{V vs NHE} \end{aligned} \tag{2}$$

$$\begin{aligned} &H_2O_2\ (aq) + 2H^+ \\ &2H_2O + 2\ h^+ \\ &E_{red}\ =\ 1.76\ \text{V vs NHE.} \end{aligned} \tag{3}$$

The overall reactions are correspondingly

$$\begin{aligned} &CH_3OH\ (aq) + 1/2\ O_2\ (g) \\ &H_2CO\ (aq) + H_2O + 2e^- + 2\ h^+ \\ &E_{redox}\ = 1.43\ \text{V} \end{aligned} \tag{4}$$

$$\begin{aligned} &CH_3OH\ (aq) + H_2O_2\ (aq) \\ &H_2CO\ (aq) + 2H_2O + 2e^- + 2\ h^+ \\ &E_{redox}\ = 1.96\ \text{V.} \end{aligned} \tag{5}$$

In terms of the electron and hole currents chemically induced by the direct and cross reactions, the equations describing the conduction band and valence band current densities $j_{c,i}$ and $j_{v,i}$ for the fuel oxidation ($i=f$) and oxidizer reduction ($i=o$) reactions are given by:[20]

$$j_{c,i} = j^0_{c,i}\left[1 - \exp\left(\frac{E_{fc} - E_i}{KT}\right)\right] \tag{6}$$

and

$$j_{v,i} = -j^0_{v,i}\left[1 - \exp\left(-\frac{E_{fv} - E_i}{KT}\right)\right] \tag{7}$$

where $j^0_{c,i}$ and $j^0_{v,i}$ are the corresponding exchange current densities obtained from[20] as:

$$j^0_{c,i} = ek_{0,i}N_c c_{red,i}\exp\left[-\frac{(E_c - E_i + \lambda)^2}{4KT\lambda}\right] \tag{8}$$

$$j^0_{v,i} = ek_{0,i}N_v c_{ox,i}\exp\left[-\frac{(E_v - E_i - \lambda)^2}{4KT\lambda}\right]. \tag{9}$$

In Eqs. (8) and (9), k_0 is the rate constant of the reaction, $N_c$and N_v are density of states of the conduction and valence band, respectively, $c_{red,i}$ and $c_{ox,i}$ are the concentrations of the reduced and oxidized species of the fuel or the oxidizer, respectively. Equations (6–7) clearly demonstrate that the decisive factor for the direction of the net current flow for each reaction is the location of the semiconductor quasi-Fermi level with respect to the redox potential. This is in contrast to the most common approximation used by the semiconductor electrochemistry community, where the band edge positions are directly used to calculate the currents, instead of using the quasi-Fermi levels directly arising from the Gerischer's model for the semiconductor/solution interface charge transfer.[22]

In our configuration the pn-junction and the applied voltage bias enable us to control the Fermi level separation in the device, and it therefore becomes necessary to consider the full Gerischer picture. To establish the fundamental limits for the charge injection from redox reactions, we formulate the

Table 1. Parameters and representative values used in describing the properties of the GaAs cell in contact with methanol and oxygen or hydrogen peroxide.

Parameter	Value	Ref.
methanol oxidation energy (E_M)	−4.3 eV vs vacuum	[18]
oxygen reduction energy (E_{O2})	−5.73 eV vs vacuum	[6]
hydrogen peroxide reduction energy (E_{H2O2})	−6.25 eV vs vacuum	[19]
rate constant at zero current (k_0)	1×10^{-17} $cm^4\,s^{-1}$	[20]
concentration of reduced (c_{red}) and oxidized (c_{ox}) species	1 M	-
density of states in GaAs conduction band (N_c)	4.7×10^{17} (cm^{-3})	[20]
density of states in GaAs valence band (N_v)	7×10^{18} (cm^{-3})	[20]
GaAs conduction band edge energy ($E_{c,GaAs}$)	−4.07 eV vs vacuum	[21]
GaAs valence band edge energy ($E_{v,GaAs}$)	−5.5 eV vs vacuum	[21]

steady state conditions of the system, requiring that charge accumulation at the conduction and valence bands of the semiconductor is suppressed. With the sign convention in Eqs. (6-9) this leads to requiring that

$$j_{c,f} + j_{c,o} - j_R = 0 \tag{10}$$

$$j_{v,f} + j_{v,o} + j_R = 0 \tag{11}$$

where j_R is the current term accounting for the combined effect of recombination of the injected charge carriers and the current flowing through an external circuit. This model allows extracting the performance limits for 1) the idealized open circuit voltage, 2) the idealized short-circuit current of the system and 3) the overall quantum efficiency of the system under selected simplifying approximations.

The ideal open circuit voltage condition corresponds to the situation where no recombination within the semiconductor nor conduction through an external circuit occurs, i.e. $j_R = 0$. In this case the quasi-Fermi levels for non-degenerate conditions can be obtained as

$$E_{fc} = E_f + kT \ln\left(\frac{j^0_{c,f} + j^0_{c,o}}{j^0_{c,f} + j^0_{c,o}\exp\left(\frac{E_f - E_o}{KT}\right)}\right) \tag{12}$$

$$E_{fv} = E_o - kT \ln\left(\frac{j^0_{v,f} + j^0_{v,o}}{j^0_{v,o} + j^0_{v,f}\exp\left(\frac{E_f - E_o}{KT}\right)}\right). \tag{13}$$

Considering GaAs, methanol, hydrogen peroxide (or oxygen) as the semiconductor, fuel and oxidizer in this model and using the corresponding parameter values (presented in Table 1), E_{fc} and E_{fv} in $CH_3OH + H_2O_2$ and $CH_3OH + O_2$ systems were calculated as a function of λ. The results are shown in Figure 3(a). With small values of reorganization energy ($\lambda <$ 0.25 eV for $CH_3OH + H_2O_2$ and $\lambda < 0.5$ eV for $CH_3OH + O_2$) the quasi-Fermi level positions align with the energy levels of the fuel and oxidizer, respectively. This clearly violates the assumption of non-degeneracy, but nevertheless shows that in principle, the thermodynamics itself can allow quasi-Fermi separations reaching at least the non-degenerate limit, even though non-radiative recombination could certainly limit the separation already earlier. When the reorganization energy increases, the rates of the cross reactions start to increase and limit the quasi-Fermi level splitting and the efficiency. There is uncertainty in the value for the reorganization energy of methanol in liquid and vapor phases, but for typically reported values of the reorganization energy λ, the quasi-Fermi level splitting can be quite large, as shown in inset of Figure 3(a). For instance, at λ~1.1 eV and λ~0.65 eV, which have been reported for methanol-based systems in Refs,[25,26] quasi-Fermi level splitting of approximately 1.1 and 1.2 eV is expected for a $CH_3OH + H_2O_2$ system, respectively, under the ideal open circuit condition. Similarly, for the $CH_3OH + O_2$ system the values would be 1.0 and 1.15 eV. According to works of Marcus,[27] the solution reorganization energy could be even smaller at semiconductor electrodes, leading to still slightly larger predictions for the quasi-Fermi level splitting.

Under ideal short circuit current condition, no Fermi level splitting takes place and E_{fc} and E_{fv} are kept at their equilibrium values. The currents $j_{c,f}$ and $j_{v,o}$ associated with the direct reactions are directly given by Eqs. (6–7) and limited to the values set by the exchange currents. The currents $j_{v,f}$ and $j_{c,o}$ associated with the cross reactions, on the other hand, are not bound by the exchange currents but depend exponentially on the biases. Nevertheless, under short circuit conditions their magnitude is negligible with respect to the direct currents, as seen by studying the reaction efficiencies for the oxidation and reduction reactions. The reaction efficiencies, defined as the ratios of the direct reactions to the sum of direct and cross reactions, i.e.

$$\eta_f = j_{c,f}/(j_{c,f} + j_{v,f}) \tag{14}$$

and

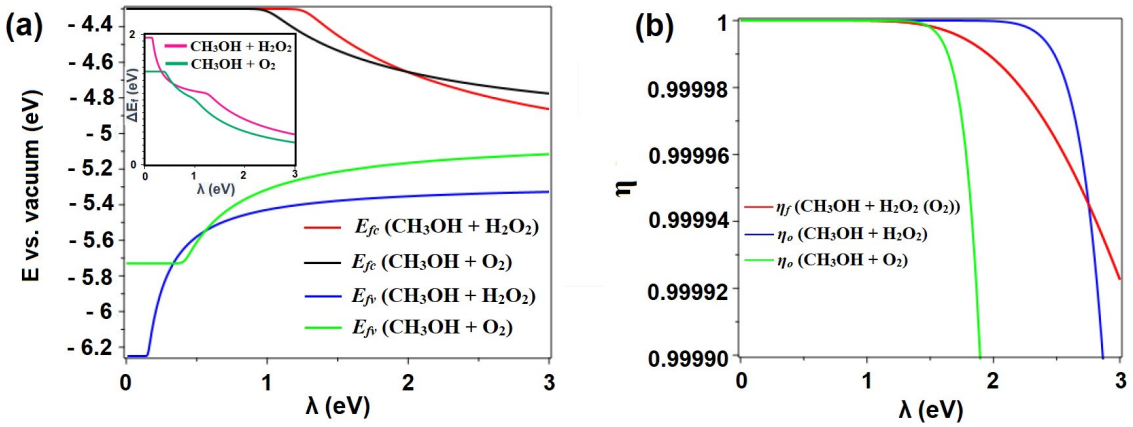

Figure 3. (a): Calculated quasi-Fermi levels of the electrons and holes for GaAs in contact with $CH_3OH + H_2O_2$ and $CH_3OH + O_2$ solutions as a function of reorganization energy under ideal open circuit conditions. **(b)**: fuel oxidation and oxidizer reduction reaction efficiencies as a function of reorganization energy in contact with $CH_3OH + H_2O_2$ and $CH_3OH + O_2$ solutions under ideal short-circuit conditions. The inset in **(a)** shows the corresponding quasi-Fermi level separation ΔE_f.

$$\eta_o = j_{v,o}/(j_{c,o} + j_{v,o}) \quad (15)$$

represent the fraction of the fuel (oxidizer) reactions that lead to the generation of an excited electron or a hole in the system. The η_f and η_o as a function of λ in contact with a nearly intrinsic GaAs ($E_{fc} = E_{fv} = -4.5$ eV vs, vacuum) under short-circuit conditions are presented in Figure 3 (b). Under these conditions, η_f and η_o for both $CH_3OH + H_2O_2$ and $CH_3OH + O_2$ systems are essentially 1 meaning that no cross-reactions are expected to occur. In other words, in the short circuit case, the electrons resulting from fuel oxidation are only injected to the conduction band of the semiconductor, whereas the oxidizer reaction captures electron only from the valence band.

The overall efficiency of the system, defined as $\eta_t = j_R/j_{tot}$ with $j_{tot} = j_{c,f} + j_{v,f} = -(j_{c,o} + j_{v,o})$ and j_R having the meaning defined earlier, is related to the reaction efficiencies through

$$\eta_t = j_R/j_{tot} = (j_{c,f} + j_{c,o})/(j_{c,f} + j_{v,f}) = (\eta_f + \eta_o) - 1 \quad (16).$$

where Eq. (10) was first used to relate j_R to $j_{c,f}$ and $j_{c,o}$, and then $j_{c,o}$ was written as $-(j_{tot} + j_{v,o})$ and is finally related to η_f and η_o using Eqs. (14) and (15). Overall, Eq. (16) shows that the maximum overall quantum efficiency $(\eta_t = 1)$ is reached when the reaction efficiencies for the oxidation and reduction reactions add up to 2 ($\eta_f = \eta_o = 1$). This was seen as the typical case for the short circuit condition. Also, the overall efficiency of the system reaches the minimum $(\eta_t = 0)$ for the ideal open circuit condition where $j_R = 0$. Under these conditions, the reaction efficiencies for the oxidation and reduction reactions add up to 1 ($\eta_f + \eta_o = 1$), meaning that at least one of the reactions is dominated by the cross reaction component. Interestingly, even though at least one of the oxidation and reduction reactions involved in these systems is preferably occurring through cross reactions to the opposite semiconductor band, the quasi-Fermi level splitting is still substantial, as shown in Figure 3(a) presenting the open circuit voltage.

The model suggests that the open-circuit voltage (V_{oc}) of a semiconductor chemovoltaic cell induced from chemical excitation can be high, indicating the potential for efficient energy conversion in the system. Also, the model highlights that the short-circuit current (J_{sc}) is primarily determined by the exchange currents, emphasizing their importance in achieving high performance. On the other hand, while the model provides valuable insights, it is important to consider that the practical performance of the system depends on various parameters beyond the simplified model. These parameters may include fuel properties, system design, operating conditions, and other factors such as recombination which can influence the actual Fermi level splitting and the efficiency of the fuel oxidation and oxidizer reduction reactions.

3. Results

The fundamental thermodynamics and our previous experimental results using silicon as a fuel[28,29] clearly suggest that chemical excitation of semiconductors is possible when suitable redox couples are present and have electrode potentials that straddle the *quasi-Fermi levels* of the semiconductor. To substantiate this prediction in practice with renewable fuels in vapor and liquid phase, we carried out several experiments resulting in chemical excitation and current production in GaAs based chemovoltaic cells. The devices themselves were GaAs/GaInP pn hetero-junctions fabricated by metal-organic vapor phase epitaxy (MOVPE), and due to this structure, they can also work as photovoltaic devices. In GaAs-based systems, we expect the base materials to exhibit at least moderate stability in aqueous environments, given that the inherent stability window defined by the separation of the relevant decomposition potentials of GaAs are normally quoted to be approximately in the range of 0.5–0.7 V.[30] Hence, GaAs may be stable in aqueous solutions up to ~0.5–0.7 V excitation. It also possesses the capability to readily host other III–V materials on its surface, providing it with an advantage over silicon based devices in this study; In contrast to GaAs, Si is quite unstable and starts to oxidize as soon as it is exposed to air or an aqueous solution.[31]

Figure 4 displays a schematic picture of the main experimental setups where the GaAs-based chemovoltaic system is in contact with a liquid or vapor phase methanol fuel. The devices

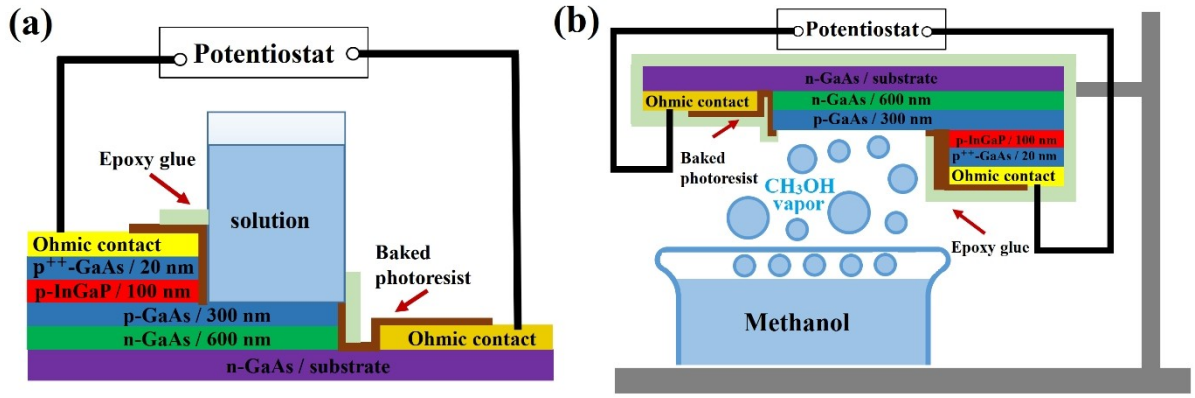

Figure 4. Schematic side view diagram of the GaAs chemovoltaic cell with **(a)** liquid and **(b)** vapor phase operation.

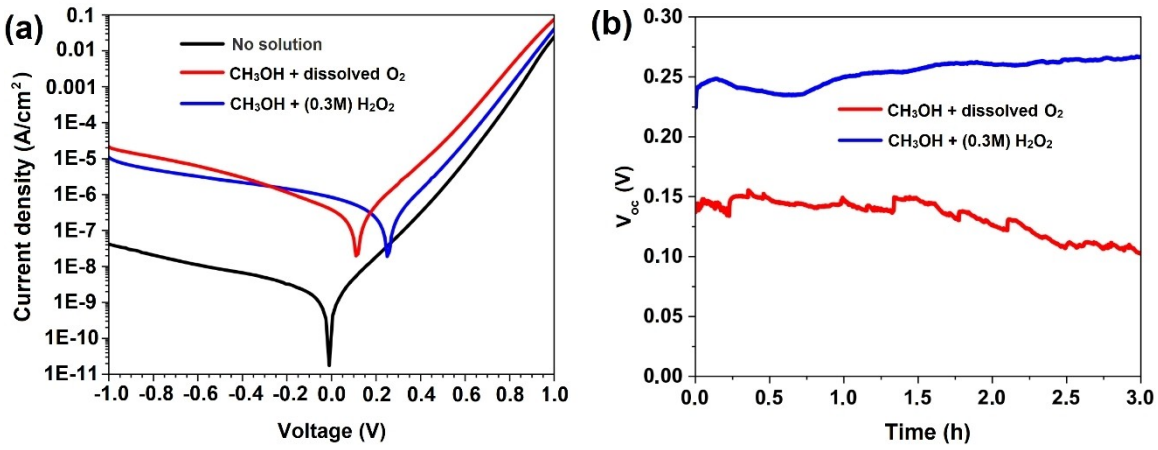

Figure 5. (a): I–V curves of the GaAs cell in the dark with and without exposure to CH_3OH or CH_3OH + (0.3 M) H_2O_2 and **(b)**: Chronopotentiometry curve of the GaAs cell exposed to CH_3OH or CH_3OH + (0.3 M) H_2O_2.

are fully encapsulated except for a surface region on top of the pn-junction that is left in contact with the non-ionic solution or vapor (see Methods section for more details). The measurements were carried out using CH_3OH and $CH_3OH + H_2O_2$ solutions (with different concentrations of the fuel and oxidizer), as well as CH_3OH vapor. Similar results have also been observed for ethanol (liquid phase) and H_2 (vapor phase, generated while the sample was submerged in an electrolyte), but only the results for the experiments involving methanol are discussed in more detail in this work.

3.1 Liquid fuel

Figure 5(a) shows the J–V results of the system in complete darkness before and after filling the glass pipe acting as a fuel compartment with different fuel and oxidizer solutions. In the dark, V_{oc} and I_{sc} in the absence of a fuel are zero as expected. When either CH_3OH (+ dissolved O_2) or CH_3OH + (0.3 M) H_2O_2 is introduced in the fuel pipe, the cell generates a V_{oc} of 125 and 250 mV and an I_{sc} of 0.4 and 0.9 μA/cm^2, respectively, clearly showing that the e-h system has been driven out of equilibrium and has the capability to produce energy through the pn-junction. It is worth noting that no significant change was observed in the J–V results compared to the dark condition when only H_2O_2 or water was introduced into the pipe. Figure 5(b) further shows the results of a three-hour chronopotentiometry test that was carried out at a fixed current of 0 A in CH_3OH (+ dissolved O_2) or CH_3OH + (0.3 M) H_2O_2 solutions under absolute darkness to investigate the stability of the device. A reasonably constant and continuous electricity generation can be observed in the presence of the CH_3OH solution within the first 1.5-hour of the measurement. Despite minor fluctuations, the V_{oc} does not change significantly. However, by the end of the 3-hour measurement, the V_{oc} has dropped by 25% compared to its initial value. For $CH_3OH + H_2O_2$ solution, the V_{oc} almost immediately reaches 250 mV and after a slight decrease to 235 mV within 30 min, it slightly increases throughout the remaining 2.5 hours of the measurement.

The J–V and V-t tests were also conducted with varying concentrations of fuel and oxidizer to comprehensively verify the results. These results are shown in the Supplementary material, but the main conclusions are described here. When methanol is diluted by adding water to the solution, V_{oc} decreases as the CH_3OH:H_2O ratio decreases (see fig. S1(a)). Specifically, V_{oc} decreases to 120 mV, 110 mV, and 70 mV for the ratios of 3:1, 1:1, and 1:3, respectively. Similarly, varying the H_2O_2 concentration yields comparable outcomes. At a low molarity of 0.05 M, V_{oc} remains similar to the V_{oc} of the $CH_3OH + O_2$ system. However, as the oxidizer concentration is increased to 0.1 M, the measured V_{oc} of the cell rises to around 200 mV.

During a 30-minute chronopotentiometry measurement of the diluted $CH_3OH + O_2$ system, the open circuit voltage experiences a drop of 10%, 15%, and 28% for the lightly diluted (CH_3OH:H_2O (3:1)), the stoichiometric (CH_3OH:H_2O (1:1)), and highly diluted (CH_3OH:H_2O (1:3)) solutions, respectively (see fig. S1(b)). Chronopotentiometry tests were also conducted in CH_3OH + (0.1 M) H_2O_2 and CH_3OH + (0.05 M) H_2O_2 solutions for 30 minutes. At the end of the measurement, the V_{oc} has decreased by 3% and 5% compared to its initial maximum value for the 0.1 M and 0.05 M solutions, respectively. The introduction of water into the methanol solution generally reduces the generated voltage and can also hinder the fuel and oxidizer molecules from reaching the semiconductor surface and inducing excitation.[32] Conversely, substituting water with hydrogen peroxide enhances the oxidation reactions and improves the overall performance of the system.

3.2 Vapor fuel

The single reaction surface of the chemovoltaic effect introduces interesting possibilities to explore whether alternative operating modes for the reactions can also be found. Figure 6 shows the J–V results of the GaAs diode under absolute

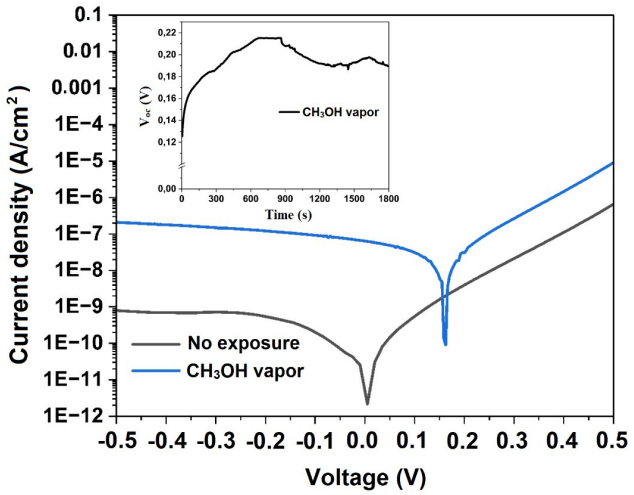

Figure 6. I–V curves of the GaAs cell in the dark when exposed to CH_3OH vapor. The inset shows the chronopotentiometry curve of the GaAs electrode under CH_3OH vapor exposure.

darkness with and without exposure to methanol vapor. The un-exposed diode shows a standard rectifying curve with V_{oc} and J_{sc} of zero. However, when the diode is exposed to methanol vapor evaporating from the container below it, the J–V characteristics show an obvious electrical response with a V_{oc} of 160 mV and an I_{sc} of 65 nA/cm^2. This indeed demonstrates that the chemovoltaic effect and possibility to convert chemical energy to electricity also exists for gas/vapor fuels. The chronopotentiometry result, presented in the inset of Figure 6, reveals an average voltage of ~180 mV during a 30-minute period of exposure to CH_3OH vapor. The V_{oc} peaks at 210 mV after the first 15 minutes and then gradually decreased and saturates at 190 mV possibly due to reaching the steady state for the methanol vapor as a result of the solution and vapor flow stabilization.

The solar cell performance of the studied GaAs device is shown in the Supplementary material (see fig. S2). Under uncalibrated flashlight illumination with modest intensity and no chemical bath, the cell produced an open circuit voltage (V_{oc}) of 660 mV and short circuit current (J_{sc}) of 60 μA/cm^2 (fig. S2). The relatively low open circuit voltage is likely related with strong surface recombination and the fairly thin 300 nm buffer layer between the device layers and the interface between the substrate and the device layers.

4. Discussion

This work shows that next to conventional fuel cells, which rely on two electrodes, ionic conduction, and semipermeable membranes, it is possible to envision devices that require none of these and offer a possibility for versatile energy conversion even through gas phase reactions. The performance of these devices directly depends on the practically available values of the reorganization energy and rate constants of the reactions, which directly influence the energy conversion efficiency as well as the achievable power densities. On the other hand, the possibility of gas phase reactions and surface engineering can open new possibilities for new catalysts and hybrid devices capable of efficient operation in both chemical and photovoltaic processes. However, estimating the efficiency of energy conversion or charge extraction would require more sophisticated combined measurements of the reaction products and currents, and these call for follow-up studies that may be challenging due to the small reaction rates in the present device.

The chemical activity of the semiconductor surface and available catalysts directly influence the current densities through the exchange current densities in Eqs. (6–9), with the maximum rate of the direct reactions primarily set by the exchange current. The impact of catalyst has been recently investigated by our group where, to our knowledge, the concept that is closest to the current study was used to report electricity generation via metal assisted chemical etching of a Si-based p-n junction in HF + H_2O_2 solution.[28] In the work it was found that the presence of a catalyst increases the short circuit current density by several orders of magnitude, while without the catalyst it has the same order of magnitude as in the current work.[28] The typical value for exchange current density can vary significantly depending on the specific reaction, electrode material, and experimental conditions. For instance, He et. al.,[33] have reported a value of 0.5–4 mA/cm^2 for exchange current density of ultrathin Pt shells deposited on palladium-based nanocubes when catalyzing the hydrogen evolution reaction (HER) in an alkaline solution. In our case, one may expect that such values give an order of magnitude as well, but in reality, the achievable values of exchange current densities remain unknown, especially for the vapor phase reactions. Exploring and optimizing catalyst materials and surface morphology for the semiconductor chemovoltaic devices can nevertheless lead to significant improvements in electricity generation during exposure to fuel, as compared to the values observed in this work.

The chemovoltaic model presented above showed that at the limit of low recombination rates, the chemically induced quasi-Fermi level separation could lead to non-degenerate carrier densities (see Figure 3 (a) and (b)). With more realistic conditions the separation will strongly depend on the actual recombination or current extraction rates, but it could nevertheless exceed the decomposition potentials of plain GaAs that are determined by cathodic and anodic decomposition potentials. These are expected to be separated by at most 0.7 eV in aqueous environments.[30] While it is possible to artificially limit the output voltage by the external load so that the quasi-Fermi levels don't exceed the decomposition potentials it is also possible to envision that the device surfaces can be passivated against decomposition. Such passivation layers could prevent direct contact between the semiconductor and the solution and provide chemical protection of the semiconductor from unwanted oxidation and corrosion. This passivation layer could also be extremely thin (nanometer scale or even a monolayer) to allow charge tunneling through it unless a passivating

semiconductor with similar band gap and small band offsets is found.

One of the main parameters affecting the magnitude of the cross reactions is the reorganization energy which consequently has a pivotal role on the achievable efficiency of the energy conversion. However, the mechanism determining the reorganization energy can be very different in liquid and vapor phases where e.g., the permittivities of the environment can be vastly different (e.g. typically 1 for vapors, 30 for methanol and 80 for water[34]). In vapor/gas-phase processes, reorganization energy can thus influence reaction rates and activation energies but may have wildly different magnitudes and limitations as compared to the liquid phase.

In the best case, the gas phase reactions can provide an attractive test environment for the reactions, with simpler dynamics than the liquid phase reactions where the number of molecules encircling the reactions is substantially larger than in the liquid phase. This might make them more tractable also for first principle calculations. Even with some potentially simpler elements, however, the exact reaction steps and mechanisms in vapor phase, the impact of external conditions on the charge transfer process, are currently not known and call for further work. In principle the same applies to the liquid phase reactions, but in their case the earlier works on semiconductor electrochemistry can provide more direct experimental precedence also for the chemovoltaic cells.

Overall, this work opens up an opportunity to explore an alternative avenue for using renewable fuels, beyond fuel cells by reporting the effect of chemovoltaic power generation using GaAs pn-juntions and by providing a semi-quantitative model to explain the observed reactions based on well-established semiconductor electrochemistry models. For future studies and optimizations, the kinetics will nevertheless be extremely relevant and more extensive exploration of the charge transfer kinetics and thermodynamics at the interface between the semiconductor and the solution can further expand the scope of energy conversion, enabling the utilization of a broad spectrum of chemical compounds for energy generation. In future follow-up studies, more detailed reactions, reaction steps, and alternative reaction pathways, extending beyond the energy overlaps of the Gerischer model, are also required to elaborate the charge transfer mechanism associated with the chemovoltaic effect. While this work obviously focuses on the fundamental thermodynamic aspects of the chemovoltaic effect on semiconductors, the next steps and technological possibilities will depend significantly on whether suitable catalysts and optimizations can be implemented to increase the reaction rates and achieved voltages. If breakthroughs in these areas are achieved, then the possibility to combine fuel cell like systems with solar cells not only diversifies the related research fields but also provides alternative avenues for sustained electricity production throughout the entire day. In parallel, the chemovoltaic effect could also allow the development of new types of gas sensors.

5. Conclusions

We developed a thermodynamic charge transfer model for describing the chemovoltaic effect of renewable fuels on semiconductor surfaces and demonstrated that the redox reactions of a fuel and an oxidizer on the surface of a photovoltaic cell can indeed chemically excite the semiconductor. The excitation leads to a Fermi level splitting for the conduction and valence bands, which allows the direct conversion of chemical energy to electricity when the GaAs surface of the PV cell is exposed to liquid or vapor phase methanol in the presence of oxygen or hydrogen peroxide. The demonstrated chemovoltaic cell provides the possibility to develop solar cells that are fed by chemical energy, in addition to the development of versatile fuel cells capable of converting non-ionic biofuels (such as alcohols or even sugars) and vapor-phase fuels into electricity. More thorough understanding of the energy conversion process and its prospects nevertheless calls for additional efforts on optimizing the system, on improving the cell design, and on exploring the relevant materials and catalysts. Practical implementations of such chemovoltaic cells can eventually function as hybrid chemovoltaic/photovoltaic cells, ideally providing access to autonomous all-day power supplies with a possibility for internal chemical energy storage and conversion.

Experimental Section

The chemovoltaic cells used to study the chemovoltaic energy conversion were prepared using GaAs/GaInP pn double heterojunctions cells grown by metal-organic vapor phase epitaxy (MOVPE) technique. The grown layer structures shown in Figure 4 consisted of a highly doped 300 nm-thick GaAs buffer layer ($n = 3\times10^{18}\,cm^{-3}$) on an n-type GaAs substrate, followed by GaAs pn junction with doping density of $1\times10^{18}\,cm^{-3}$ and thickness of 300 nm for both the n- and p-layer. The p-type GaAs layer was finally followed by a 100 nm – thick p-type GaInP barrier layer doped by Zn to $4\times10^{17}\,cm^{-3}$ and a highly doped p^{++}-type GaAs cap layer (20 nm, doping concentration $2\times10^{19}\,cm^{-3}$) to decrease leakage current of the device and to allow better ohmic contacts, respectively. After epitaxy and for liquid measurement, the device mesas consisting of two 2 mm-diameter circles connected with a narrow (100×2100 μm) bridge, were fabricated by maskless aligner photolithography and wet chemical etching (see fig. S3 (a)). One of the circles formed the active area and another served as a contact pad, connected to the active area through the bridge area. The etchant solutions used for etching were the mixtures of H_3PO_4:H_2O_2:H_2O (3:1:25) and HCl:H_2O (3:2) for GaAs and GaInP etching, respectively. Metal contacts were deposited on the p^{++} cap layer using a vacuum electron beam evaporation system, with Au (100 nm)/Ti (30 nm) bilayer films covering the contact pad, the bridge, and the outer rim of the active area, whereas AuGe (110 nm)/ Ni (10 nm) thin film electrode was deposited on the entire area of the n-type substrate outside the mesas. The devices were annealed using rapid thermal annealing technique at $T = 350\,^{\circ}C$ for $t = 15$ s. Next, the two topmost layers (GaAs cap and GaInP barrier layers) were etched from the active area between the contact circle in another lithography step so that the topmost surface of the p-GaAs layer in the pn junction became exposed as an active area. Finally, the device was encapsulated with a photoresist heated at 200 °C for 2 h except for the opening

revealing the junction area in the active mesa and the contact pad to ensure that only the opened areas would be in contact with the solutions. The exposed surface of the active area was passivated by 7 M HCl solution to remove the possible oxide layer formed during encapsulation step. For the liquid fuel measurement, a glass pipe with a 2 mm inner diameter and 2 cm length was attached as the fuel compartment on the active area of the device using epoxy glue. For the vapor phase fuel measurement, similar processing steps were employed, with the only difference being that the mesa area was much larger (~0.4 cm^2), and two wires were attached to p and n contacts using silver paste (see fig. S3(b)). Additionally, the entire area of the device (except the active area) was covered with epoxy glue. The electrochemical measurements were conducted with different solutions in the pipe including methanol (CH_3OH) and different concentration of CH_3OH, namely H_2O: CH_3OH (3 : 1), H_2O:CH_3OH (1 : 1) and H_2O: CH_3OH (3 : 1). The measurement was also carried out by adding 0.3, 0.1 and 0.05 M hydrogen peroxide (H_2O_2), as an alternative oxidizer, to CH_3OH. The vapor phase measurement was performed by holding the prepared device above (~1 cm distance) a beaker filled with methanol. The electrical properties of the device were characterized with conventional I–V and chronopotentiometry measurements.

Acknowledgements

The authors gratefully acknowledge the financial support by the Academy of Finland [Grants No. 1502005 and 348754], and the provision of facilities and the technical support by the Micronova Nanofabrication Centre at Aalto University.

Conflict of Interests

The authors declare no conflict of interest.

Data Availability Statement

Research data are not shared.

Keywords: Chemovoltaic effect · Semiconductor solar cells · Electrolyte-free fuel cell · GaAs diode · Renewable chemical energy

[1] J. D. White, J. Chen, D. Matsiev, D. J. Auerbach, A. M. Wodtke, *Nature* **2005**, *433*, 503–505.
[2] B. Gergen, H. Nienhaus, W. H. Weinberg, E. W. McFarland, *Science* **2001**, *294*, 2521–2523.
[3] S. W. Lee, *Trends Chem.* **2023**.
[4] M. M. Montemore, R. Hoyt, G. Kolesov, E. Kaxiras, *ACS Catal.* **2018**, *8*, 10358–10363.
[5] J. Y. Park, S. M. Kim, H. Lee, I. I. Nedrygailov, *Acc. Chem. Res.* **2015**, *48*, 2475–2483.
[6] A. Fujishima, K. Honda, *Nature* **1972**, *238*, 37–38.
[7] J. Tan, B. Kang, K. Kim, D. Kang, H. Lee, S. Ma, G. Jang, H. Lee, J. Moon, *Nat. Energy* **2022**, *7*, 537–547.
[8] T. S. Teitsworth, D. J. Hill, S. R. Litvin, E. T. Ritchie, J.-S. Park, J. P. Custer Jr, A. D. Taggart, S. R. Bottum, S. E. Morley, S. Kim, *Nature* **2023**, *614*, 270–274.
[9] J. Qin, J. Barrio, G. Peng, J. Tzadikov, L. Abisdris, M. Volokh, M. Shalom, *Nat. Commun.* **2020**, *11*, 4701.
[10] P. Ding, T. Jiang, N. Han, Y. Li, *Materials Today Nano* **2020**, *10*, 100077.
[11] L. Wan, Q. Zhou, X. Wang, T. E. Wood, L. Wang, P. N. Duchesne, J. Guo, X. Yan, M. Xia, Y. F. Li, *Nature Catalysis* **2019**, *2*, 889–898.
[12] S. Kattel, P. J. Ramírez, J. G. Chen, J. A. Rodriguez, P. Liu, *Science* **2017**, *355*, 1296–1299.
[13] X. Yang, S. Kattel, S. D. Senanayake, J. A. Boscoboinik, X. Nie, J. Graciani, J. A. Rodriguez, P. Liu, D. J. Stacchiola, J. G. Chen, *J. Am. Chem. Soc.* **2015**, *137*, 10104–10107.
[14] F. A. Chowdhury, M. L. Trudeau, H. Guo, Z. Mi, *Nat. Commun.* **2018**, *9*, 1707.
[15] Y. A. Wu, I. McNulty, C. Liu, K. C. Lau, Q. Liu, A. P. Paulikas, C.-J. Sun, Z. Cai, J. R. Guest, Y. Ren, *Nat. Energy* **2019**, *4*, 957–968.
[16] H. Zhao, R. Yu, S. Ma, K. Xu, Y. Chen, K. Jiang, Y. Fang, C. Zhu, X. Liu, Y. Tang, *Nature Catalysis* **2022**, *5*, 818–831.
[17] T. Takata, J. Jiang, Y. Sakata, M. Nakabayashi, N. Shibata, V. Nandal, K. Seki, T. Hisatomi, K. Domen, *Nature* **2020**, *581*, 411–414.
[18] Z. Liu, Z. Yin, C. Cox, M. Bosman, X. Qian, N. Li, H. Zhao, Y. Du, J. Li, D. G. Nocera, *Sci. Adv.* **2016**, *2*, e1501425.
[19] Y. Shiraishi, Y. Ueda, A. Soramoto, S. Hinokuma, T. Hirai, *Nat. Commun.* **2020**, *11*, 3386.
[20] R. Memming, *Semiconductor electrochemistry*, John Wiley & Sons, **2015**.
[21] S. S. Sarkar, S. Bera, M. S. Hassan, S. Sapra, R. K. Khatri, S. K. Ray, *J. Phys. Chem. C* **2021**, *125*, 10768–10776.
[22] H. Gerischer, *Solar energy conversion: Solid-state physics aspects* **2005**, 115–172.
[23] H. Gerischer, *Electrochim. Acta* **1990**, *35*, 1677–1699.
[24] H. Gerischer, *J. Electroanal. Chem. Interfacial Electrochem.* **1983**, *150*, 553–569.
[25] D. V. Matyushov, *Chem. Phys.* **1993**, *174*, 199–218.
[26] A. Hazra, A. V. Soudackov, S. Hammes-Schiffer, *J. Phys. Chem. B* **2010**, *114*, 12319–12332.
[27] R. A. Marcus, *J. Phys. Chem.* **1990**, *94*, 1050–1055.
[28] S. Li, K. Chen, V. Vähänissi, I. Radevici, H. Savin, J. Oksanen, *J. Phys. Chem. Lett.* **2022**, *13*, 5648–5653.
[29] S. Li, H. M. Ayedh, M. Yli-Koski, V. Vähänissi, H. Savin, J. Oksanen, *J. Phys. Chem. C* **2023**, *127*, 4072–4078.
[30] S. Chen, L.-W. Wang, *Chem. Mater.* **2012**, *24*, 3659–3666.
[31] N. T. Plymale, M. Dasog, B. S. Brunschwig, N. S. Lewis, *J. Phys. Chem. C* **2017**, *121*, 4270–4282.
[32] R. Rincón, F. J. García-Vidal, F. Flores, *Appl. Surf. Sci.* **1996**, *92*, 216–221.
[33] T. He, W. Wang, F. Shi, X. Yang, X. Li, J. Wu, Y. Yin, M. Jin, *Nature* **2021**, *598*, 76–81.
[34] M. Mohsen-Nia, H. Amiri, B. Jazi, *J. Solution Chem.* **2010**, *39*, 701–708.

Manuscript received: October 20, 2023
Revised manuscript received: January 7, 2024
Accepted manuscript online: February 2, 2024
Version of record online: February 16, 2024